A flow law for pseudotachylytes in the continental crust

François X. Passelègue[1,2], Jacob Tielke[3,4,5], Julian Mecklenburgh[2], Marie Violay[1], Damien Deldicque[6], Giulio Di Toro[2,7]

[1] *Laboratoire Expérimental de Mécanique des Roches, École Polytechnique Fédérale de Lausanne, Switzerland*

[2] *School of Earth and Environmental Sciences, The university of Manchester, England*

[3]*University of Liverpool, Liverpool, England.*

[4]*Lunar and Planetary Institute, Houston, Texas.*

[5] *Astromaterials Research and Exploration Science*, Houston, Texas.

[6]*Laboratoire de Géologie de l'École Normale Supérieure, Paris, France.*

[7]*Dipartimento di Geoscienze, Università degli Studi di Padova, Italy*

ABSTRACT

While the plastic strength of individual minerals constituting the continental crust are well known, the plastic strength of rocks resulting from co-seismic slip in seismically active regions has yet to be measured, despite of the observations of their plastic reactivation during the inter-seismic period. We establish the flow law parameters controlling the strength of natural pseudotachylyte, fine grained fault rocks that crystalize from melt produced in fault zones during earthquakes. Experiments where conducted at temperature ranging from 700° to 900°C and at a confining pressure of 300 MPa. Our results demonstrate that pseudotachylyte deforms via diffusion creep at crustal conditions. Flow law parameters derived from plastically-deforming pseudotachylyte suggest that the presence of pseudotachylyte along faults drastically reduces the strength of the seismically-active continental crust. Finally, the presence of seismically-generated pseudotachylyte are

likely to strongly influence the thickness of the seismogenic layer, since seismicity is rare in mature crustal faults at depths below which pseudotachylyte deforms plastically.

INTRODUCTION

The seismogenic layer spans the range of depths within the crust in which most earthquakes nucleate and propagate (Brace & Byerlee, 1970; Scholz, 1998). The thickness of this layer (from 40 to 60 km and from 10 to 25 km for continental and oceanic crust, respectively) (Watts & Burov, 2003), varies at different locations, and is expected to be controlled by (i) the composition of the crust (ii) the age of the crust (Jackson et al., 2008), and (iii) the geodynamic context of the area (Fig. 1A). The strength of the crust is commonly modelled using the laboratory measurements of the strength of quartz, feldspars or olivine (Tullis & Yund, 1992; Hirth & Tullis, 1994; Darot et al., 1985; Kohlstedt et al., 1995), and lower boundary of the continental seismogenic zone is limited by the onset of crystal-plastic deformation of these mineralsThese deformation mechanisms such as dislocation and diffusion creep, become active with increasing temperature and water content. Experimental studies also highlight the importance of grain size dependent diffusion creep (Kronenberg & Tullis, 1984), as well as the role of partial melting (Mecklenburgh & Rutter, 2003) and the presence of glass (Violay et al., 2012) in controlling strain localisation and the strength of the lithosphere (Kirby, 1985; Jaroslow et al., 1996; Platt & Behr, 2011).

Based on these experiments, the interseismic plastic flow at depth, controlling the elastic loading of a fault, is extrapolated from visco-elastic modelling using flow laws derived from experimental studies conducted on monomineralic (e.g., quartz, feldspar) rock assemblages representative of the crust at depth (Tullis & Yund, 1992; Hirth & Tullis, 1994, Darot et al.,

1985; Kohlstedt et al., 1995). However, the strength of the crust and the plastic flow along fault zone could be controlled by both microstructure and polycrystalline assemblage of the localized shear zone. For instance, we know that seismic ruptures may propagate at depth forming pseudotachylytes along faults due to frictional heating (Fig. 1A and B) (Fig. 1B) (Reilinger et al., 2000; Handy & Brun, 2004; Wright et al., 2013). Recent field observations highlighted that these pseudotachylytes are reactivated plastically (Fig. 1D) (Passchier, 1982; Pennacchioni & Cesare, 1997; Menegon et al., 2017), suggesting that the deformation at depth in the plastic domains could be largely accommodated by the localized sheared zone, and controlled by their microstructures. Despite all of these observations, the onset of the solid-state viscous deformation of pseudotachylytes as well as the implications of their presence at depth on the strength of the continental crust remains poorly constrained (Rabinowitz et al., 2011). To address these issues, we present the results of creep experiments conducted on natural pseudotachylytes under crustal conditions. This study aims at answering to the following questions: Under what conditions do pseudotachylytes veins deform plastically? How the presence of pseudotachylytes affects the hypocentral depth of earthquakes and the strength of the continental crust?

METHODS AND RESULTS

The samples used in this study are from the Gole Larghe Fault Zone which cuts the tonalites of the Adamello massif (Italian Alps: Di Toro & Pennacchioni, 2006). Three types of rocks were used in deformation experiments: (i) intact tonalite (host rock of the fault zone), (ii) intact pseudotachylyte collected from centimetres-thick fault veins, and (iii) tonalite samples containing 20 to 100 micrometer-thick tabular pseudotachylytes veins oriented at 45 ^{o} to the direction of maximum compressive stress (Figs. 2 and S1). Creep experiments were conducted at

71 a confining pressure of 300 MPa and temperatures of 700, 800, and 900 ^{o}C in a
72 Paterson/ANUtech gas medium apparatus (Paterson, 1990) (Figs. S2 and S3) at the University of
73 Manchester.

74 Successful experiments on tonalite were carried out at 800 and 900 ^{o}C. Experiments
75 were attempted at 700 ^{o}C, but required too large applied stresses to deform via crystal-plastic
76 deformation for resolvable strain rates. At 800 ^{o}C, stress steps ranging from 60 to 249 MPa
77 yielded axial strain rates of 1.1 x 10^{-6} to 4 x 10^{-6} s^{-1} (Fig. 2A). At 900 ^{o}C, stress steps ranging
78 from 15 to 130 MPa yielded strain rates of 1.5 x 10^{-6} to 1.5 x 10^{-5} s^{-1} (Fig. 2A).

79 Intact pseudotachylyte samples were deformed at 700 to 900 ^{o}C. At 700 ^{o}C, stress steps
80 ranging from 2.7 to 200 MPa yielded strain rates of 1.2 x 10^{-6} to 6.5 x 10^{-6} s^{-1}, which are
81 comparable in strength to the results obtained on tonalite at 800 ^{o}C (Figs. 2A and 2B). Intact
82 pseudotachylyte deformed at 800 ^{o}C and at stress steps ranging from of 20 to 231 MPa yielded
83 strain rates of 1.6 x 10^{-5} to 1.8 x 10^{-4} s^{-1}. At 900 ^{o}C the strength of the material becomes very low,
84 with stress steps ranging from of 1.2 and 28.1 MPa yielding to strain rates ranging from 4.5 x 10^{-5}
85 to 1.1 x 10^{-3} s^{-1} (Fig. 2B).

86 Steady state viscous deformation of tabular pseudotachylyte veins was observed at all
87 the investigated temperatures. At 700 ^{o}C, pseudotachylyte veins sustained stresses ranging from
88 10 to 184 MPa, yielding to shear strain rates ranging from 2.8 x 10^{-6} to 6.5 x 10^{-5} s^{-1}. At these
89 conditions, the strain rate dependence on stress follows a power-law relationship with a stress
90 exponent (n) of 1 (Fig. 2C). At 800 ^{o}C pseudotachylyte veins sustained stress steps ranging from
91 4 to 90 MPa, yielding to shear strain rates ranging from 1.2 x 10^{-5} to 7.5 x 10^{-4} s^{-1}. Note that at
92 this temperature, the highest shear stresses deviate from Newtonian behavior, consistent with an
93 increase of the stress exponent from 1 to 3, which may suggest the activation of different

94 deformation mechanisms (Fig. 2C). At 900 °C, the pseudotachylyte vein becomes very weak and
95 its plastic behaviour does not follow a simple power-law relationship. Moreover, the
96 pseudotachylyte vein sustained a maximum stress step of only 11 MPa, yielding to a strain rate
97 of 1.2 x 10^{-3} s^{-1} (Fig. 2C), highlighting the relative weakness of the sheared vein.

98 As common practice in high-temperature experimental rock deformation, mechanical
99 data obtained at not realistic ambient temperatures (>700 °C) and strain rates (10^{-6} s^{-1}) were
100 extrapolated to a larger range of geophysical conditions by determining the flow law parameters.
101 The strain rate $\dot{\gamma}$ resulting from plastic processes at a given stress can be written as

$$\dot{\gamma} = \dot{A e^{\frac{E_a}{RT}} \tau^n}$$

102 with A the pre-exponent factor (including the grain size dependence), E_a the activation energy of
103 the deformation mechanism, n the stress exponent, T the bulk temperature and R the gas
104 constant.

105 We solved for flow law parameters (E_a and A) by minimizing the sum of the residuals
106 using a least-squares method for both diffusion and dislocation creep mechanisms (Fig. S3). The
107 results of the least squares fit are in excellent agreement with the measured mechanical
108 behaviour as exemplified in Fig. 2C. According to our mechanical data inversion analysis, the
109 activation energy for diffusion creep (E_a^{diff}=193 kJ/mol) is much smaller than for dislocation
110 creep (E_a^{disl}=793 kJ/mol), suggesting that diffusion creep is expected to be the dominant
111 deformation mechanism within the conditions of the seismic to aseismic transition in nature.
112
113 **MICROSTRUCTURES**
114 Intact tonalite exhibits evidence of brittle processes at all temperatures tested.
115 Conversely, SEM analysis on intact pseudotachylytes revealed localized deformation in

116 experiments conducted at 800 °C (Fig. 3A). At a given distance from the localized zone,
117 pseudotachylyte included domains that are typical of the starting natural pseudotachylyte (Fig.
118 1C). In the high-strain domains, EBSD analyses reveal the occurrence of a crystallographic
119 preferred orientation for plagioclase (Fig. S4), interpreted as resulting from the rotation of the
120 plagioclase microlites (Fig. S4). Analyses of pseudotachylyte veins highlight that the strain is
121 accommodated within the veins and the host tonalite remains undeformed (Fig. 3D). The grains
122 constituting the recrystallised pseudotachylyte reveal very little evidence of recrystallization and
123 crystal-plastic (i.e., dislocation) processes (Fig. 3E) despite the large shear strain sustained in the
124 veins (γ=5), in agreement with the weak preferential crystallographic orientation revealed by
125 EBSD analysis (Fig. S5). Isolated domains with glassy-like structures similar to those shown in
126 (Fig. 3C) were found in the samples sheared at 800 and 900 °C. However, we infer that (i) the
127 amount of melt produced in the shear zone during these high temperature experiments was low
128 (melt fraction < 1% in surface area from image analysis (Fig. S6)) and (ii) that the melt pockets
129 are not inter-connected at 800 °C, indicating that melting will have limited effect on the observed
130 mechanical behaviour in experiments on pseudotachylyte veins at 800 °C. As a consequence, the
131 flow law parameters (activation energy, stress exponent, etc.) were inverted only from the
132 experimental data obtained at 700 and 800 °C.
133
134 **INTERPRETATION AND DISCUSSION**
135 Previous studies reporting experiments conducted at room temperature suggested that
136 pseudotachylytes produced in the shallow (>12 km depth) continental crust could induce an
137 increase of the post-slip strength of faults (Proctor & Lockner, 2016; Mitchell et al., 2016). This
138 strengthening is explained by the welding of the slip surface during melt quenching. Very few

139 experiments have been conducted at higher temperatures on pseudotachylytes so far (Rabinowitz
140 et al., 2011; Proctor et al., 2017). Our experimental results demonstrate that deeper in the
141 continental crust (i) solid-state viscous deformation of pseudotachylytes is systematically
142 observed in the range of pressure and temperature tested (Fig. 3) and (ii) pseudotachylytes are
143 much weaker than the host rock and localize deformation (Figs. 2-3).

144 Our experimental results are in agreement with the solid-state viscous deformation of
145 pseudotachylyte bearing rocks observed in nature (Passchier, 1982; Pennacchioni & Cesare,
146 1997; Menegon et al., 2017) (Fig. 1D). While the finite strain achieved during experiments
147 remains relatively small compared to natural case, experiments conducted on intact
148 pseudotachylytes at temperature > 800 ^{o}C highlight initiation of mylonitisation processes, with
149 notable deformation-induced shape preferred orientation of feldspar as well as the development
150 of wings on porphyroclasts composed of recrystallised quartz and feldspar (Figs. 3A and C).
151 However, little evidence of crystal-plastic deformation is observed in the pseudotachylyte veins
152 samples compared to the initial material because diffusion creep is the dominant mechanism
153 operating during solid-state viscous deformation of veins.

154 While results obtained from experiments conducted on intact pseudotachylytes
155 highlight the weakness of the material, partial and very local melting (glassy-like pods) at the
156 contact between biotite and quartz is observed in samples from experiments conducted at 800
157 and 900 ^{o}C. In these experiments, partial melting could be at the origin of the enhancement of the
158 strain-rate compared to intact tonalite. In intact pseudotachylyte, intracrystalline plasticity is
159 likely to contribute insignificantly to the observed deformation. However, this is not the case for
160 tabular pseudotachylyte veins. Only small and not interconnected melt pockets are observed,
161 suggesting that local melting does not contribute significantly to strain accommodation and

localization. These results suggest that the steady-state viscous deformation of pseudotachylyte veins is controlled by solid-state plastic processes and, based on the lack of crystallographic preferred orientation in quartz and feldspar, mostly by diffusion creep. Furthermore, over the majority of the investigated conditions the inferred stress exponent is unity.

Extrapolating our experimentally-derived flow laws to natural conditions gives insight into the strength of the continental lithosphere in actively deforming regions. Assuming regular strain-rates (Kohlstedt et al., 1995) (10^{-14} s^{-1}) and geothermal gradient for continental crust (Jackson et al., 2008; McKenzie et al., 2005), our experimental results demonstrate that the brittle to crystal-plastic transition of pseudotachylyte bearing rocks occurs at shallower depth than for micas (Mariani et al., 2006), wet quartz (Gleason & Tullis, 1995) and feldspar (Rybacki & Dresen, 2004), which are the dominant minerals of the continental crust (Fig. 4). These results suggest that pseudotachylytes formed coseismically are likely to control the strength of individual faults and that the presence of pseudotachylyte within fault zone reduces the strength of the system. The low strength of pseudotachylytes (based on the flow law parameters presented here) compared to mica-rich and granitoid rocks could also play a key role in the after slip in large earthquakes observed within the brittle crystal-plastic transition (Fig. 1B) (Reilinger et al., 2000; Handy & Brun, 2004; Wright et al., 2013).

Our mechanical data well explain strain localization within mylonitised pseudotachylytes in nature (Fig. 1D). So why are mylonitised pseudotachylytes are overprinted by new generations of pseudotachylytes? While our results indicate that nucleation of instability could be inhibited due to the weakness of pseudotachylytes, it is unlikely with regard to rupture propagation. The release of the elastic strain during subsequent seismic cycle is likely to occur through the propagation of fast ruptures, nucleating at shallower depth where the fault remains brittle. These

ruptures are expected to propagate at depth because of the large strain-rate which promotes the transition to brittle mechanisms (Fig. 4), overprinting a new generation of pseudotachylytes in the mylonitised fault zone. Finally, while rupture propagation remains possible for earthquakes nucleating in the brittle domains, the plastic reactivation of pseudotachylyte could contribute to the offset of seismicity in nature since earthquakes are rare at depths below which pseudotachylyte deforms plastically (Figure 4).

Acknowledgments

FXP acknowledges the Swiss National Science Foundation grant PZENP2/173613, GDT and FXP the ERC grant 614705 NOFEAR and JM and JT the NERC grant NE/M000087/1. Authors thanks Experimental officer Stephen May for assistance with specimen fabrication and equipment maintenance, and Dr. Mark Zimmerman for assisting with designing high-temperature furnaces. This work benefits from invaluable discussions with E. Rutter. Authors thanks an anonymous reviewer during a first round of review for his enthusiasm regarding our work.

REFERENCES

207 Brace, W. F., & Byerlee, J. D., 1970, California earthquakes: Why only shallow focus?. Science,
208 168(3939), 1573-1575.
209 Byerlee, J., 1978, Friction of rocks: In Rock friction and earthquake prediction (pp. 615-626).
210 Birkhäuser, Basel.
211 Darot, M., Gueguen, Y., Benchemam, Z., & Gaboriaud, R., 1985, Ductile-brittle transition
212 investigated by micro-indentation: results for quartz and olivine: Physics of the Earth and
213 Planetary Interiors, 40(3), 180-186.
214 Di Toro, G., & Pennacchioni, G., 2004, Superheated friction-induced melts in zoned
215 pseudotachylytes within the Adamello tonalites (Italian Southern Alps): Journal of
216 Structural Geology, 26(10), 1783-1801.
217 Di Toro, G., Hirose, T., Nielsen, S., Pennacchioni, G., & Shimamoto, T., 2006, Natural and
218 experimental evidence of melt lubrication of faults during earthquakes: Science,
219 311(5761), 647-649.
220 Frost, H. J., & Ashby, M. F., 1982, Deformation mechanism maps: the plasticity and creep of
221 metals and ceramics: Pergamon press.
222 Gleason, G. C., & Tullis, J., 1995, A flow law for dislocation creep of quartz aggregates
223 determined with the molten salt cell: Tectonophysics, 247(1-4), 1-23.
224 Handy, M. R., & Brun, J. P., 2004, Seismicity, structure and strength of the continental
225 lithosphere: Earth and Planetary Science Letters, 223(3-4), 427-441.
226 Hirth, G., & Tullis, J., 1994, The brittle-plastic transition in experimentally deformed quartz
227 aggregates: Journal of Geophysical Research: Solid Earth, 99(B6), 11731-11747.

228 Hirth, G., & Kohlstedt, D. L., 1995, Experimental constraints on the dynamics of the partially
229 molten upper mantle: Deformation in the diffusion creep regime: Journal of Geophysical
230 Research: Solid Earth, 100(B2), 1981-2001.
231 Jackson, J., McKenzie, D. A. N., Priestley, K., & Emmerson, B., 2008, New views on the
232 structure and rheology of the lithosphere: Journal of the Geological Society, 165(2), 453-
233 465.
234 Jaroslow, G. E., Hirth, G., & Dick, H. J. B., 1996, Abyssal peridotite mylonites: implications for
235 grain-size sensitive flow and strain localization in the oceanic lithosphere:
236 Tectonophysics, 256(1-4), 17-37.
237 Kirby, S. H., 1985, Rock mechanics observations pertinent to the rheology of the continental
238 lithosphere and the localization of strain along shear zones: Tectonophysics, 119(1-4), 1-
239 27.
240 Kohlstedt, D. L., Evans, B., & Mackwell, S. J., 1995, Strength of the lithosphere: Constraints
241 imposed by laboratory experiments: Journal of Geophysical Research: Solid Earth,
242 100(B9), 17587-17602.
243 Kronenberg, A. K., & Tullis, J., 1984, Flow strengths of quartz aggregates: grain size and
244 pressure effects due to hydrolytic weakening: Journal of Geophysical Research: Solid
245 Earth, 89(B6), 4281-4297.
246 Mariani, E., Brodie, K. H., & Rutter, E. H., 2006, Experimental deformation of muscovite shear
247 zones at high temperatures under hydrothermal conditions and the strength of
248 phyllosilicate-bearing faults in nature: Journal of Structural Geology, 28(9), 1569-1587.
249 McKenzie, D., Jackson, J., & Priestley, K., 2005, Thermal structure of oceanic and continental
250 lithosphere: Earth and Planetary Science Letters, 233(3-4), 337-349.

Mecklenburgh, J., & Rutter, E. H, 2003, On the rheology of partially molten synthetic granite: Journal of Structural Geology, 25(10), 1575-1585.

Menegon, L., Pennacchioni, G., Malaspina, N., Harris, K., & Wood, E., 2017, Earthquakes as precursors of ductile shear zones in the dry and strong lower crust: Geochemistry, Geophysics, Geosystems, 18(12), 4356-4374.

Mitchell, T. M., Toy, V., Di Toro, G., Renner, J., & Sibson, R. H., 2016, Fault welding by pseudotachylyte formation: Geology, 44(12), 1059-1062.

Passchier, C. W., 1982, Pseudotachylyte and the development of ultramylonite bands in the Saint-Barthelemy Massif, French Pyrenees: Journal of Structural Geology, 4(1), 69-79.

Paterson, M. S., 1990, Rock deformation experimentation. The Brittle-Ductile Transition in Rocks: Geophys. Monogr. Ser, 56, 187-194.

Pennacchioni, G., & Cesare, B., 1997, Ductile-brittle transition in pre-Alpine amphibolite facies mylonites during evolution from water-present to water-deficient conditions (Mont Mary nappe, Italian Western Alps): Journal of Metamorphic Geology, 15(6), 777-791.

Platt, J. P., & Behr, W. M., 2011, Grainsize evolution in ductile shear zones: Implications for strain localization and the strength of the lithosphere: Journal of Structural Geology, 33(4), 537-550.

Proctor, B., & Lockner, D. A., 2016, Pseudotachylyte increases the post-slip strength of faults: Geology, 44(12), 1003-1006.

Proctor, B. P., Lockner, D. A., Lowenstern, J. B., & Beeler, N. M., 2017, Conversion of Wet Glass to Melt at Lower Seismogenic Zone Conditions: Implications for Pseudotachylyte Creep: Geophysical Research Letters, 44(20), 10-248.

Rabinowitz, H., Skemer, P. A., Mitchell, T. M., & Di Toro, G., 2011, Experimental reactivation of pseudotachylite-bearing faulted rocks: AGU Fall Meeting Abstracts.

Reilinger, R. E., Ergintav, S., Bürgmann, R., McClusky, S., Lenk, O., Barka, A., ... & Aktug, B., 2000, Coseismic and postseismic fault slip for the 17 August 1999, M= 7.5, Izmit, Turkey earthquake: Science, 289(5484), 1519-1524.

Rybacki, E., & Dresen, G., 2004, Deformation mechanism maps for feldspar rocks: Tectonophysics, 382(3-4), 173-187.

Scholz, C. H., 1998, Earthquakes and friction laws: Nature, 391(6662), 37.

Scholz, C. H, 2019, The mechanics of earthquakes and faulting: Cambridge university press.

Tse, S. T., & Rice, J. R., 1986, Crustal earthquake instability in relation to the depth variation of frictional slip properties: Journal of Geophysical Research: Solid Earth, 91(B9), 9452-9472.

Tullis, J., & Yund, R., 1992, The brittle-ductile transition in feldspar aggregates: An experimental study: International Geophysics (Vol. 51, pp. 89-117). Academic press.

Violay, Marie, et al., 2012, An experimental study of the brittle-ductile transition of basalt at oceanic crust pressure and temperature conditions: Journal of Geophysical Research: Solid Earth 117.B3.

Watts, A. B., & Burov, E. B., 2003, Lithospheric strength and its relationship to the elastic and seismogenic layer thickness: Earth and Planetary Science Letters, 213(1-2), 113-131.

Wright, T. J., Elliott, J. R., Wang, H., & Ryder, I., 2013, Earthquake cycle deformation and the Moho: Implications for the rheology of continental lithosphere: Tectonophysics, 609, 504-523.

FIGURE CAPTIONS

Figure 1. Geological context of the study. (a) Distribution of the seismicity and thickness of the continental seismogenic layer of Earth (Jackson et al., 2008). (b) Illustration of the deformation history within the continental crust during the seismic cycle (modified from Tse & Rice (1986) and Handy et al. (2004)). Here the rupture nucleates at a depth of 7-8 km and propagates down to a depth of 22 km. Seismic rupture propagation (orange in color) in the middle crust is arrested by the limited elastic strain energy available in the plastically deforming crust. Stress relaxation drives post-seismic deformation in the middle to deep crust (green in color). Boxes C and D are typical crustal depths where fault rocks shown in Figures (c) and (d) can be found. (c) Field picture of pseudotachylyte-bearing (PST: used in the experiments of this study) faults hosted in tonalites (Gole Larghe Fault zone, Adamello Massif, Italy). Top right image: microstructure of the pseudotachylyte with clasts of quartz (Q) suspended in a matrix of plagioclase (Pl) and biotite (Bt) microlites (backscatter scanning electron microscope image). (d) Crystal-plastic deformation of pseudotachylyte fault vein hosted in continental granitic orthogneiss (Roraima, Brazil; optical microscope image, plane polarized light).

Figure 2. Mechanical data from creep experiments performed on tonalite (a), intact pseudotachylyte (b), and tabular pseudotachylyte veins (c). White, grey, and black circles correspond to experiments conducted at 700, 800, and 900 ^{o}C, respectively. The dashed grey lines in Fig. C are the flow laws for diffusion (n= 1), dislocation (n=3) creep. The black dashed line is a combination of the two mechanisms for the three investigated temperatures (See Suppl. Material). Note that C is plotted as shear stress and strain rate not differential stress and axial strain rate.

Figure 3. Backscattered electron images of plastically deformed pseudotachylyte-bearing rocks (Q= Quartz, Pl=Plagiolcase). (a) Pseudotachylyte after experiments conducted at 800 ^{o}C. Black arrows indicate the orientation of the maximum stress. (b) Microstructures in pseudotachylytes after small strain which are similar to those observed in the starting material (Fig. 1C). (c) Evidence of sigma-type tail development around quartz porphyroclasts assisted by partial melting and recrystallisation. (d) Pseudotachylyte veins after experiments conducted at 800 ^{o}C. Black arrows indicate the direction of shear. (e) Typical microstructures observed within the tabular pseudotachylyte veins after the experiment. No strong evidence of strain is observed. (f) Higher magnification image of the area in d., with an outline of a melt-bearing pocket observed after experiment conducted at 800 ^{o}C.

Figure 4. Extrapolation of our experimental results to natural conditions assuming an equivalent strain rate ranging from 10^{-15} to 10^{-13} s^{-1}. The geothermal gradient was computed from heat flux measurements (McKenzie et al., 2005). The frictional sliding criteria assumes regular friction criteria (Byerlee, 1978). Earthquake data represented by grey bars correspond to Californian seismicity (Scholz, 2002). The flow laws for muscovite (Mariani et al., 2006), wet quartz (Gleason & Tullis, 1995) and plagioclase (Rybacki and Dresen, 2004) are described by the blue domains, where each solid lines corresponds to a different strain rate (10^{-15}, 10^{-14}, and 10^{-13} s^{-1}). The experimentally-determined flow law for diffusion creep of pseudotachylyte is represented by the red curves and domain. The transition from frictional sliding to diffusion creep of pseudotachylytes is predicted to occur at a similar depth as the deepest recorded earthquakes.

Figure 1

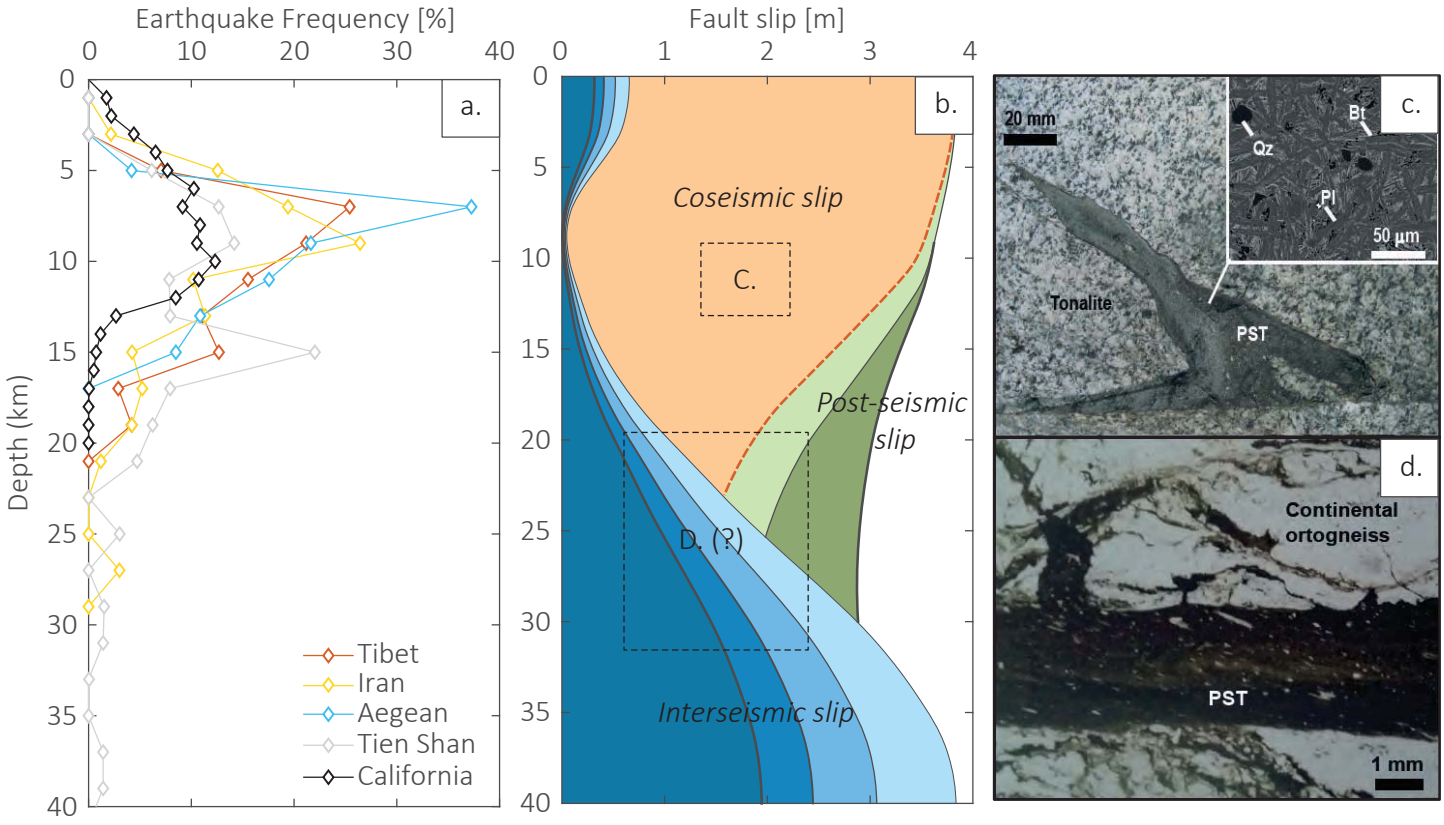
Earthquake Frequency [%]
0
10
20
30
40
a.
Depth (km)
0
5
10
15
20
25
30
35
40
Tibet
Iran
Aegean
Tien Shan
California
Fault slip [m]
0
1
2
3
4
b.
Coseismic slip
C.
Post-seismic slip
D. (?)
Interseismic slip
20 mm
c.
Qz
Bt
Pl
50 µm
Tonalite
PST
d.
Continental ortogneiss
PST
1 mm

Figure 2

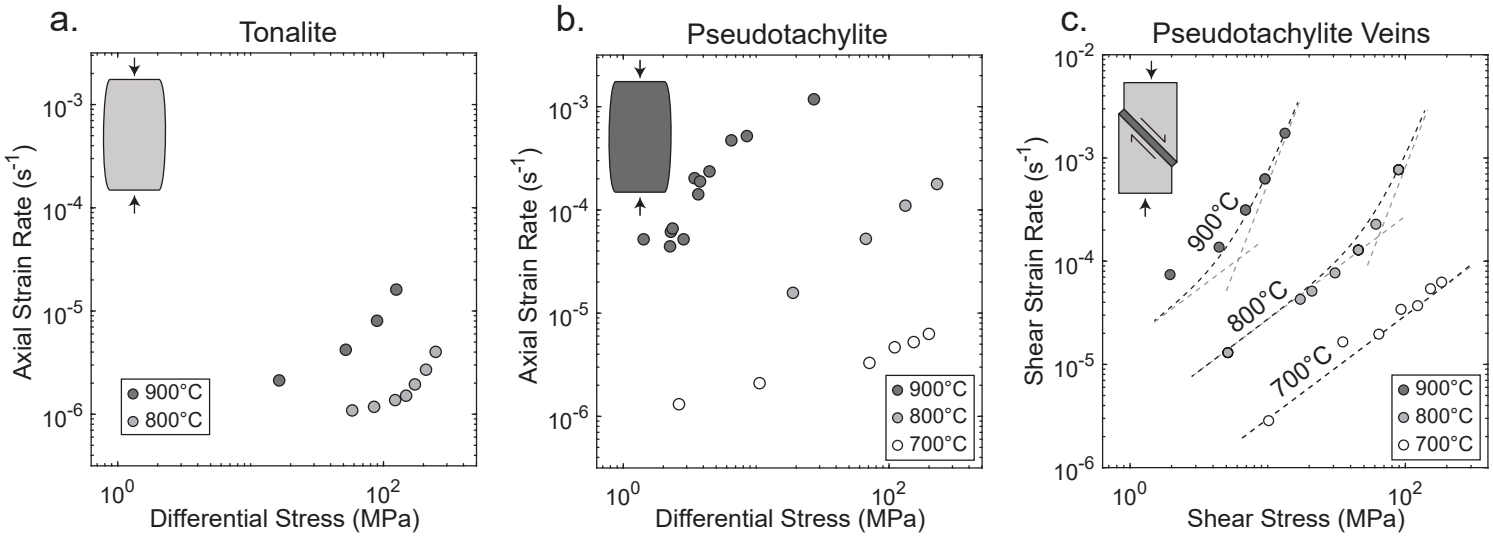
a.
Tonalite
Axial Strain Rate (s-1)
Differential Stress (MPa)
900°C
800°C
b.
Pseudotachylite
Axial Strain Rate (s-1)
Differential Stress (MPa)
900°C
800°C
700°C
c.
Pseudotachylite Veins
Shear Strain Rate (s-1)
Shear Stress (MPa)
900°C
800°C
700°C

Figure 3

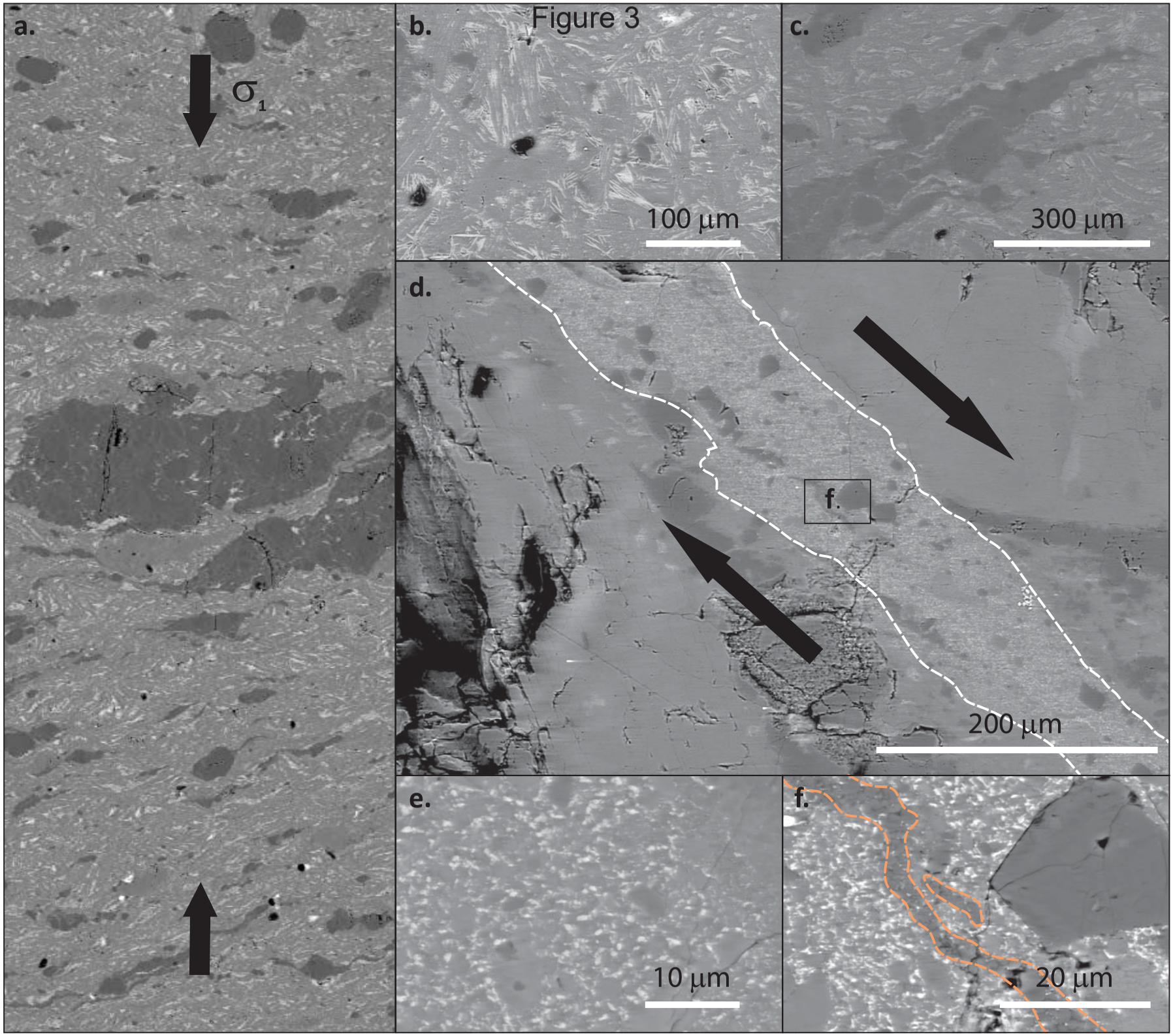

Figure 4

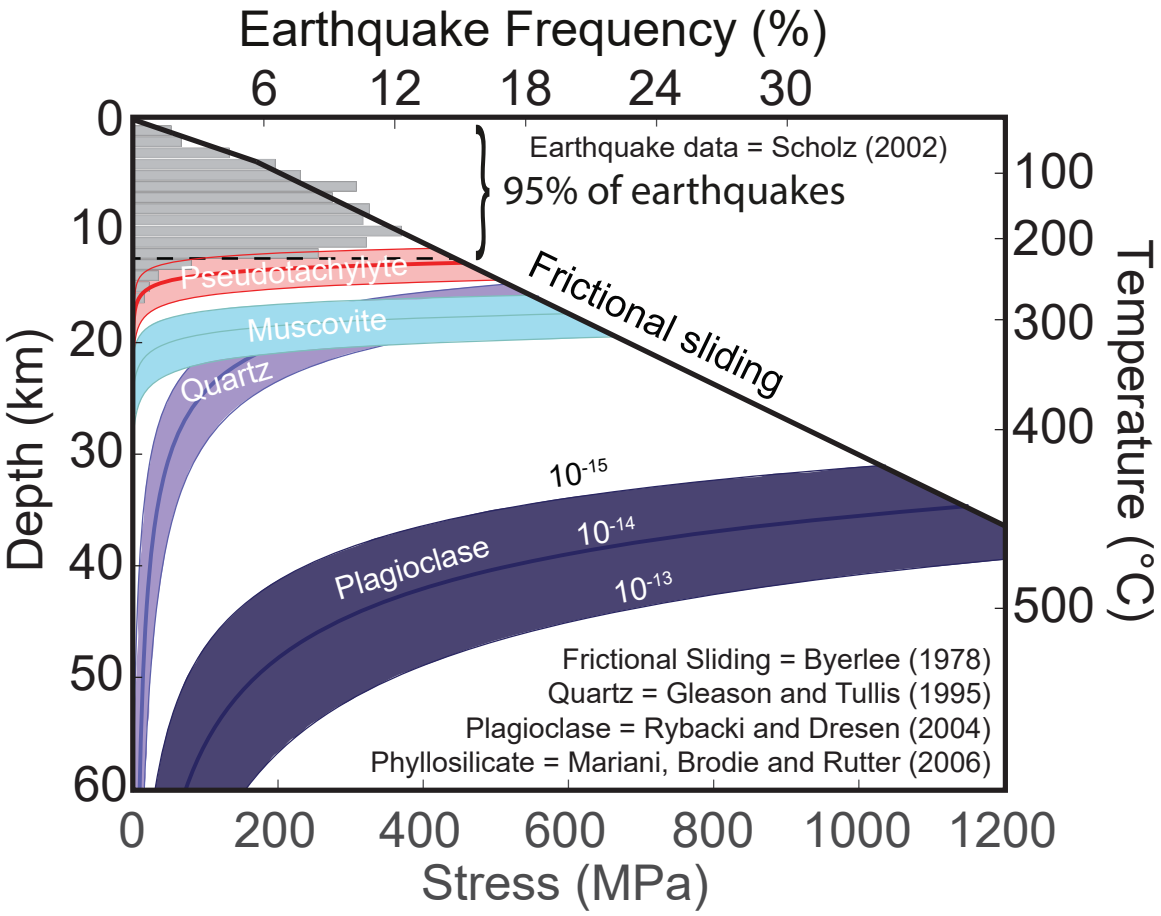
Earthquake Frequency (%)
6
12
18
24
30
0
10
20
30
40
50
60
Depth (km)
Earthquake data = Scholz (2002)
95% of earthquakes
Pseudotachylyte
Muscovite
Quartz
Frictional sliding
10^{-15}
10^{-14}
10^{-13}
Plagioclase
Frictional Sliding = Byerlee (1978)
Quartz = Gleason and Tullis (1995)
Plagioclase = Rybacki and Dresen (2004)
Phyllosilicate = Mariani, Brodie and Rutter (2006)
0
200
400
600
800
1000
1200
Stress (MPa)
100
200
300
400
500
Temperature (°C)